ARTICLE

Downregulation of CFIm25 amplifies dermal fibrosis through alternative polyadenylation

Tingting Weng[1]🄳, Jingjing Huang[1,2], Eric J. Wagner[3], Junsuk Ko[1]🄳, Minghua Wu[4]🄳, Nancy E. Wareing[1], Yu Xiang[1], Ning-Yuan Chen[1], Ping Ji[3], Jose G. Molina[1], Kelly A. Volcik[1], Leng Han[1]🄳, Maureen D. Mayes[4], Michael R. Blackburn[1], and Shervin Assassi[4]

Systemic sclerosis (SSc; scleroderma) is a multisystem fibrotic disease. The mammalian cleavage factor I 25-kD subunit (CFIm25; encoded by *NUDT21*) is a key regulator of alternative polyadenylation, and its depletion causes predominantly 3′UTR shortening through loss of stimulation of distal polyadenylation sites. A shortened 3′UTR will often lack microRNA target sites, resulting in increased mRNA translation due to evasion of microRNA-mediated repression. Herein, we report that CFIm25 is downregulated in SSc skin, primary dermal fibroblasts, and two murine models of dermal fibrosis. Knockdown of *CFIm25* in normal skin fibroblasts is sufficient to promote the 3′UTR shortening of key TGFβ-regulated fibrotic genes and enhance their protein expression. Moreover, several of these fibrotic transcripts show 3′UTR shortening in SSc skin. Finally, mice with *CFIm25* deletion in fibroblasts show exaggerated skin fibrosis upon bleomycin treatment, and *CFIm25* restoration attenuates bleomycin-induced skin fibrosis. Overall, our data link this novel RNA-processing mechanism to dermal fibrosis and SSc pathogenesis.

Introduction

Systemic sclerosis (SSc; scleroderma) is an autoimmune disease characterized by widespread skin and internal organ fibrosis. With a standardized mortality ratio of 3.5 (Elhai et al., 2012), SSc has the highest mortality among major rheumatic diseases (Elfving et al., 2014; Thomas et al., 2003). This high disease burden in SSc is driven partly by only modest response of its fibrotic features to immunosuppressive agents (Khanna et al., 2016; Tashkin et al., 2006). Mechanisms leading to the excessive fibrosis remain elusive, which has contributed to the fact that there are no US Food and Drug Administration–approved medications for skin or internal organ fibrosis in SSc. Thus, this disease remains fatal for many patients. The differentiation of myofibroblasts and the excessive production of collagen I (COL(I)) and other extracellular matrix (ECM) proteins are the pathological hallmarks of SSc skin (Bhattacharyya et al., 2011). An activation of TGFβ, a multifunctional cytokine critical for wound healing and tissue repair, has been implicated in SSc pathogenesis (Lafyatis, 2014). However, the signals responsible for the sustained activation and amplification of myofibroblasts and accumulation of ECMs are not well understood, representing a fundamental knowledge gap in our understanding of SSc pathology. Specifically, it is unknown which mediator amplification mechanisms are responsible for the exaggerated response to profibrotic cytokines.

Cleavage and polyadenylation is a pre-mRNA–processing step that completes the maturation of eukaryotic mRNAs and is required for mRNA stability, nuclear export, and efficient translation (Curinha et al., 2014). Cleavage and polyadenylation was once thought to be a constitutive process, but recent discoveries indicate this biological process is tightly regulated. In fact, a majority of mammalian genes contain more than one polyadenylation signal (PAS). Differential utilization of alternative PASs by the cleavage/polyadenylation machinery results in transcripts with variable 3′UTR tail lengths and occurs through a process known as alternative polyadenylation (APA; Di Giammartino et al., 2011; Elkon et al., 2013). Through APA, the 3′UTR length of a given mRNA can often vary in different tissues, cell cycle stages, and genetic backgrounds. In normal cells, there is a tendency for mRNAs to use a distal PAS (dPAS) located the greatest distance downstream of the stop codon. However, the proximal PAS is largely used in highly proliferating cells, leading to transcript isoforms with a shorter 3′UTR (Elkon et al., 2012; Sandberg et al., 2008). Given that the majority of human microRNAs (miRNAs) target the 3′UTR, a switch from dPAS to

[1]Department of Biochemistry and Molecular Biology, the University of Texas Health Science Center at Houston, Houston, TX;   [2]Department of Geriatrics, The Second Affiliated Hospital of Nanjing Medical University, Nanjing, China;   [3]Department of Biochemistry and Molecular Biology, The University of Texas Medical Branch at Galveston, Galveston, TX;   [4]Department of Internal Medicine, Division of Rheumatology, The University of Texas Health Science Center at Houston, Houston, TX.

Correspondence to Tingting Weng: tingting.weng@uth.tmc.edu;   Shervin Assassi: shervin.assassi@uth.tmc.edu.

proximal PAS substantially reduces the number of miRNA-binding sites (Lim et al., 2005; Linsley et al., 2007). This switch establishes a potential scenario where a shortened 3′UTR can evade miRNA-mediated gene repression and consequently increase protein expression. Over the past few years, the importance of APA has been highlighted in several pathological states, including malignancies and cardiac disorders (Creemers et al., 2016; Masamha et al., 2014; Singh et al., 2009; Soetanto et al., 2016; Tian and Manley, 2017; Xia et al., 2014).

Recently, the mammalian cleavage factor I 25-kD subunit (CFIm25; encoded by the gene *NUDT21*) was discovered as a master regulator of APA among 15 cleavage and polyadenylation factors (Gruber et al., 2012; Kubo et al., 2006; Masamha et al., 2014). However, it is unknown whether CFIm25 plays a role in the pathogenesis of skin fibrosis.

In this study, we investigated the role of the key APA regulator, CFIm25, in SSc-related dermal fibrosis. Our data demonstrated that CFIm25 levels were decreased in SSc skin and primary dermal fibroblasts. Following coimmunofluorescence and in vitro cell culture study, we further determined that CFIm25 was also downregulated in (myo)fibroblasts of fibrotic skin. Furthermore, using an unbiased, novel RNA sequencing (RNA-seq) technology, we demonstrated that depletion of *CFIm25* in dermal fibroblasts was directly associated with 3′UTR shortening and increased translation of key profibrotic genes and ECMs. Moreover, 3′UTR shortening was confirmed in several key TGFβ-regulated profibrotic genes in the SSc skin. Consistent with these findings, we also observed that genetic deletion of *CFIm25* in fibroblasts leads to increased ECM deposition in murine dermal fibrosis models, while overexpression (OE) of *CFIm25* promotes the 3′UTR lengthening of key fibrotic genes and attenuates bleomycin-induced skin fibrosis. Overall, our study systematically identified a novel role for CFIm25 and APA in SSc pathogenesis.

Results

CFIm25 is downregulated in human fibrotic skin and is selectively decreased in (myo)fibroblasts

First, we mined our previously published global gene expression data attained from arm skin biopsies from 61 SSc patients and 36 age-, gender-, and ethnicity matched controls. These data indicated that SSc patients had significantly lower *CFIm25* (gene name: *NUDT21*) mRNA level (Assassi et al., 2015; Fig. 1 A). Moreover, patients with disease duration <2 yr (representing the early and active subset of disease; Maurer et al., 2015; Steen and Medsger, 2000) had significantly lower *CFIm25* mRNA levels than late-stage patients (P = 0.009; Fig. 1 B). Next, we investigated CFIm25 expression in human skin collected from 10 SSc patients and 10 matched controls by dual immunohistochemistry. Table S1 shows the demographic and clinical characteristics of participants in the immunohistochemistry experiments. CFIm25 was ubiquitously expressed in the nucleus of the majority of the cells in normal skin (Fig. 1 C, arrowheads, red), but was decreased in α smooth muscle actin (α-SMA)–positive (α-SMA⁺) myofibroblasts in SSc skin (Fig. 1 C, arrows, green). Blinded cell counting indicated that the

percentage of CFIm25-positive (CFIm25⁺) fibroblasts was significantly decreased in SSc fibroblasts (Fig. 1 D). Further analysis showed that the majority of α-SMA⁺ cells are CFIm25 negative (Fig. S1 B) and the majority of CFIm25-negative (CFIm25⁻) cells are α-SMA positive (Fig. S1 C). Although the percentage of CFIm25⁻/α-SMA⁺ fibroblasts over total α-SMA⁺ fibroblasts was not changed in SSc skin (Fig. S1 B), the absolute number of CFIm25⁻α-SMA⁺ cells was significantly increased (Fig. 1 E). These findings suggest that CFIm25 is mainly downregulated in α-SMA⁺ cells, and it is downregulated in SSc skin possibly due to an overall increase in the number of α-SMA⁺ cells in the dermal layer. Consistent with these observations, CFIm25 protein expression was dramatically downregulated in primary fibroblasts isolated from SSc skin compared with those from normal skin (Figs. 1 F and S1 D). Together, these data show that *CFIm25* is downregulated in SSc skin and fibroblasts relative to normal skin and fibroblasts.

RNA-seq identifies important fibrotic pathways targeted by CFIm25

The functional consequence of *CFIm25* suppression on fibroblast activation and ECM production is not known. To systematically identify genes directly targeted by *CFIm25*, RNA-seq was performed to determine the global APA profile of five normal human dermal fibroblasts (HDFs) in response to *CFIm25* depletion. As shown in Fig. 2, A and B, 971 genes (8.1%) showed significant shortening in their 3′UTR in response to *CFIm25* knockdown (KD), while only 93 genes (0.7%) showed significant lengthening. Next, an unbiased Ingenuity analysis of predicted upstream regulators of the genes with shortened 3′UTRs was conducted. This analysis revealed TGFβ as the top upstream regulating growth factor/cytokine (P = 6.82 × 10⁻³), followed by angiotensinogen, Angiopoietin 2, and fibroblast growth factor (Fig. 2 C). Specifically, 97 TGFβ-regulated genes showed 3′UTR shortening upon *CFIm25* KD in dermal fibroblasts. The list of genes with shortened 3′UTRs upon *CFIm25* KD can be found on our website (https://www.uth.tmc.edu/scleroderma/).

Notably, a similar predicted upstream growth factor/cytokine analysis in our previously published large SSc skin gene expression dataset also identified TGFβ as the most activated upstream regulator (Assassi et al., 2015), supporting a link between *CFIm25* and SSc pathogenesis. Cumulatively, these data support that *CFIm25* is a key regulator of fibrotic pathways through its APA regulation in HDFs.

Removing CFIm25 is sufficient to promote profibrotic factor and ECMs expression through APA

Due to the importance of the TGFβ pathway in skin fibrosis and SSc pathogenesis (Lafyatis, 2014), we chose four CFIm25 targeted genes involved in this pathway to confirm the results of RNA-seq: *COL1A1*, *TGFBR1*, *COL11A1*, and *SPARC*. In addition, these four genes had increased transcript expression in SSc skin in our global gene expression data (Assassi et al., 2015). We first performed Western blot analysis to determine whether the protein expression of these four genes is increased altered following *CFIm25* depletion. As shown in Figs. 3 A and S2, COL(I) (including COL1A1 and COL1A2), TGFBR1, and COL11A1 showed

Weng et al.
CFIm25 mediated APA in dermal fibrosis

Journal of Experimental Medicine
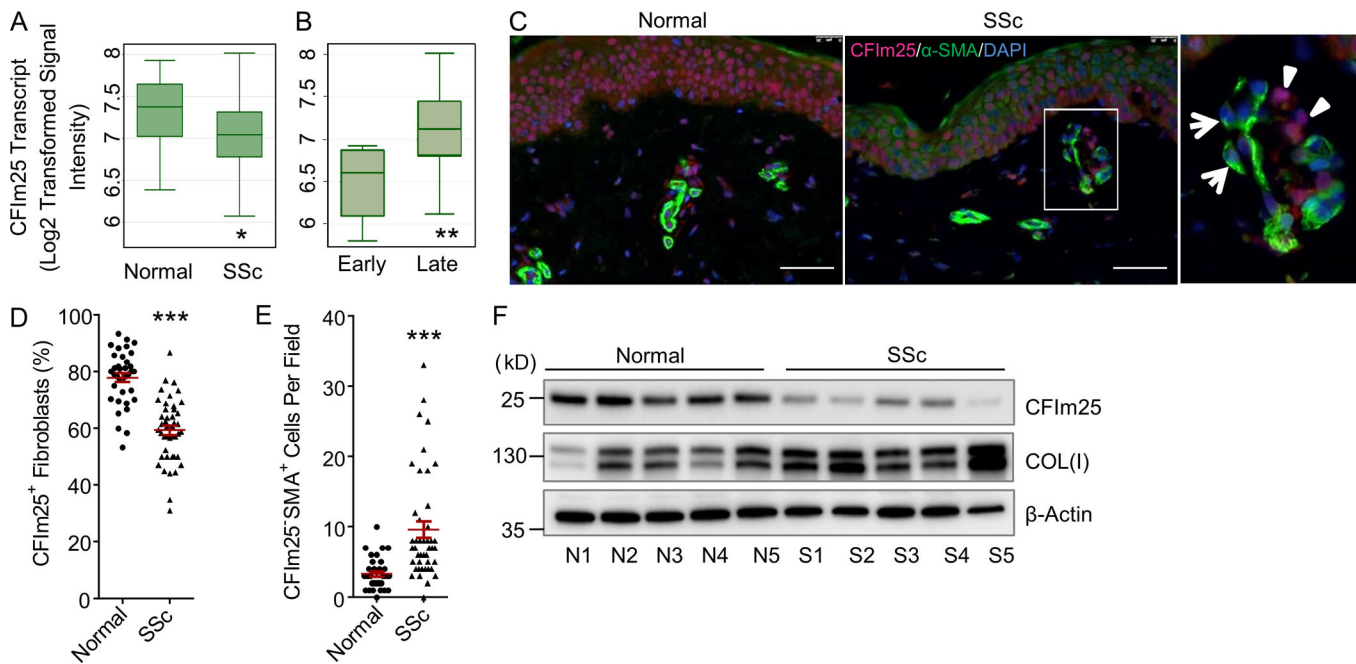https://doi.org/10.1084/jem.20181384

2

Figure 1. **CFIm25 is depleted in myofibroblasts of SSc skin. (A)** Comparison of *CFIm25* transcript levels in 61 SSc and 36 matched controls (shown as log-transformed signal intensity) indicates significant *CFIm25* downregulation in SSc. **(B)** *CFIm25* transcript levels in the skin of early and late Ssc patients (*n* = 54). The y axis in A and B indicates the log2-transformed signal intensity of *CFIm25*. Data were analyzed using a Student's *t* test. **(C)** Dual immunostainings show CFIm25 (red) and α-SMA (green) expression in normal and SSc skin (*n* = 10). Arrowheads show CFIm25-positive cells, and arrows point to myofibroblasts; nuclei are blue. Scale bars = 50 μm. **(D)** The percentage of CFIm25+ fibroblasts were counted and calculated. **(E)** The number of CFIm25− and α-SMA+ cells were counted. P value was calculated using two-tailed Student's *t* test to determine the difference between normal and SSc cells. **(F)** CFIm25 protein expression was examined in primary fibroblasts derived from five unaffected controls and five SSc patients. For A and B, data are presented as box and whisker plot showing quartiles and range. For D and E, data are mean ± SEM and representative of two experiments with *n* = 10 per group. Data were analyzed using a Student's *t* test; *, P < 0.05; **, P < 0.01; ***, P < 0.001.

enhanced protein levels in all five fibroblast cell lines, and secreted protein acidic and cysteine-rich (SPARC) protein expression was increased in four out of five fibroblasts upon successful *CFIm25* depletion (Fig. 3 A). To confirm whether the increased protein expression was resulting from APA, we next used a real-time quantitative PCR (RT-qPCR)–based method to monitor the usage of the dPAS of *COL1A1*, *TGFBR1*, *COL11A1*, and *SPARC*. Briefly, two pairs of primers were designed, with one targeting the open reading frame of transcripts to represent the total transcript level and the other targeting sequences just before the dPAS to detect long transcripts that used the dPAS (Fig. 3 B, upper panel). A normalized dPAS usage was calculated as ΔΔCT, with a negative value indicating the mRNA has 3′UTR shortening compared with the control. All four genes showed
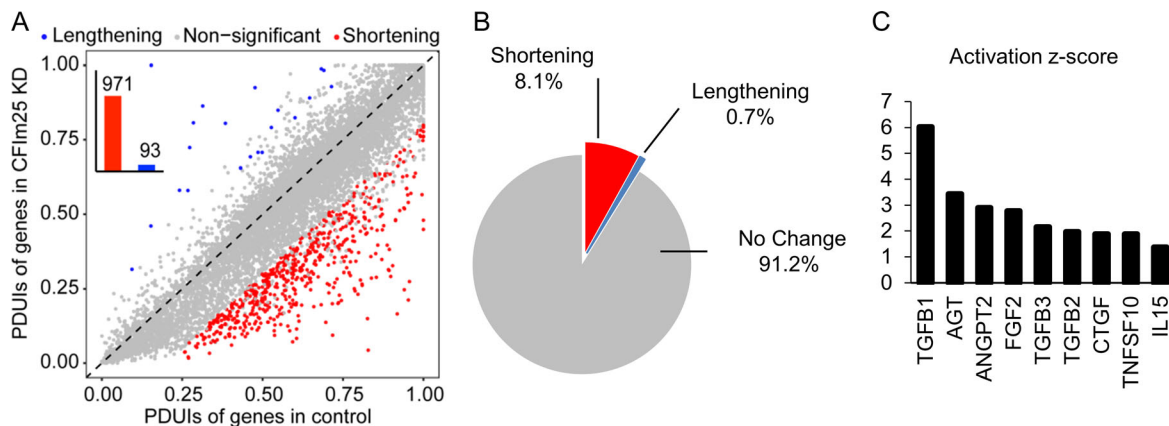

Figure 2. **RNA-seq of *CFIm25* KD versus control in normal HDFs (*n* = 5). (A)** Representative scatterplot of PDUIs in control and *CFIm25* KD cells where mRNAs are significantly shortened (*n* = 971) or lengthened (*n* = 93) after *CFIm25* KD in five HDFs. **(B)** Pie graph showing 971 (8.1%) genes had shortened 3′UTR, while only 93 (0.7%) genes showed 3′UTR lengthening. **(C)** TGF-β pathway was predicted to be the top upstream regulator of the *CFIm25* KD APA profile, followed by angiotensinogen, Angiopoietin 2, and fibroblast growth factor pathways.
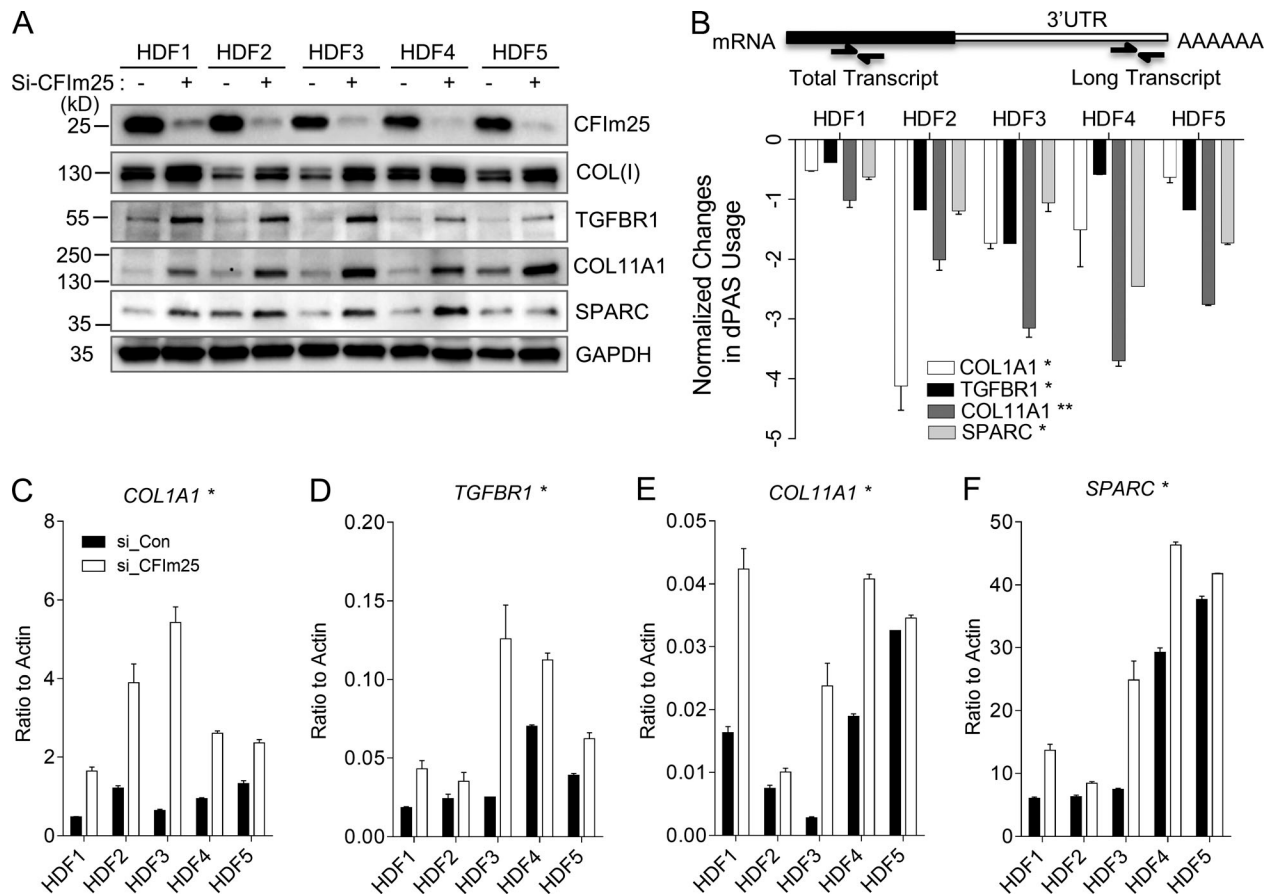
Figure 3. **KD of *CFIm25* induces APA and upregulation of fibrotic factors in normal HDFs.** Five primary normal HDFs were transfected with *CFIm25* specific siRNA (si_*CFIm25*) or a si-RNA control. **(A)** Western blot confirmed effective KD of CFIm25 and showed increased protein levels of COL(I), TGFBR1, COL11A1, and SPARC. **(B)** The upper panel demonstrates the primer locations for monitoring APA, and the lower panel demonstrates normalized dPAS usage by RT qPCR showing 3′UTR shortening upon *CFIm25* KD. **(C–F)** RT-qPCR demonstrates increased *COL1A1, TGFBR1, COL11A1,* and *SPARC* transcript levels in *CFIm25* KD HDFs. Data are mean ± SEM of n = 3 independent experiments (five primary cell lines and two biological replications). P values were determined using a one-sample t test comparing to 0 (B) or a paired two-tailed Student's t test comparing si_CFIm25 to si_Con (C–F). *, $P < 0.05$; **, $P < 0.01$.

decreased dPAS usage (i.e., 3′UTR shortening) in *CFIm25* KD fibroblasts compared with the control siRNA (Fig. 3 B, lower panel), demonstrating that depletion of *CFIm25* directly leads to the 3′UTR shortening of all four genes. Concomitant with 3′UTR shortening, the transcript levels of all four genes were increased (Fig. 3, C and D) in *CFIm25*-depleted skin fibroblasts. Taken together, these data further confirm that *CFIm25* depletion alone is sufficient to regulate APA and enhance the TGFβ pathway and COL(I) synthesis.
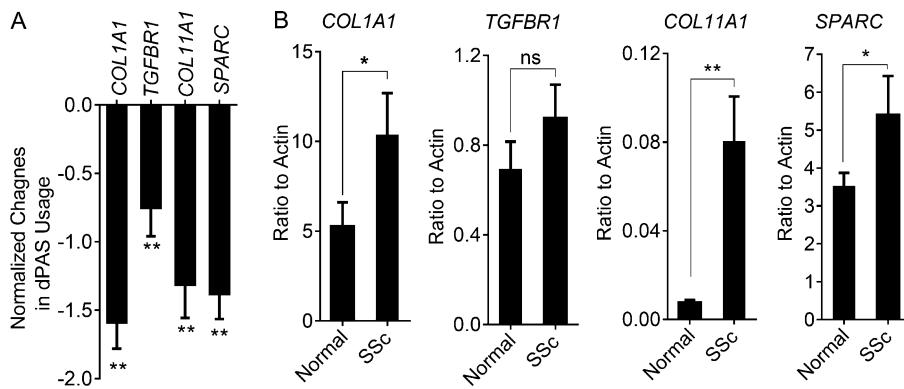
Key TGFβ-regulated fibrotic genes show 3′UTR shortening in SSc skin

The above in vitro experiments suggest that *CFIm25* depletion promotes APA of important profibrotic genes. To extend our findings to SSc skin in comparison to matched unaffected controls, we performed RT-qPCR assays in the above four, TGFβ-regulated, verified *CFIm25*-targeted genes. We conducted the dPAS usage analysis in 10 SSc-affected skin samples obtained from patients with early diffuse cutaneous involvement and 10 age- and gender-matched controls. Table S2 shows the demographic and clinical characteristics of participants in these

experiments. This analysis revealed that all four genes, *COL1A1, COL11A1, TGFBR1,* and *SPARC,* had 3′UTR shortening in SSc skin (Fig. 4 A). The overall transcript levels of *COL1A1, COL11A1,* and *SPARC* were also increased in SSc skin. Although *TGFBR1* transcript levels were numerically higher in SSc skin, this difference did not reach statistical significance (Fig. 4 B). Taken together, key *CFIm25* regulated profibrotic genes, including *COL1A1,* exhibit 3′UTR shortening in SSc skin, underscoring the potential role of this RNA-processing factor in SSc pathogenesis.

CFIm25 is downregulated in mouse skin fibrosis

We next sought to understand whether a similar mechanism was involved in mouse models of skin fibrosis in vivo. S.c. bleomycin administration is a widely used inflammation-driven dermal fibrosis model (Yamamoto and Nishioka, 2005; Yamamoto et al., 1999). In this model, 8-wk-old female mice were treated with repeated s.c. bleomycin injections (0.02 U/mice, injected six times a week for 4 wk). Mice treated with the same amount of PBS were used as controls. Similar to the findings in human tissue, CFIm25 protein expression was decreased in the skin of bleomycin-injected mice (Figs. 5 B and S3 A)

Weng et al.
CFIm25 mediated APA in dermal fibrosis

Journal of Experimental Medicine
https://doi.org/10.1084/jem.20181384

4

Figure 4. **APA of *CFIm25* targets was present in SSc skin. (A)** Normalized dPAS usage performed by RT-qPCR showing *COL1A1*, *COL11A1*, *TGFBR1*, and *SPARC* had 3'UTR shortening in affected skin collected from SSc patients. *n* = 10. **, P < 0.01 versus 0. **(B)** The transcript levels of above four genes were analyzed using RT-qPCR. Data are presented as mean ± SEM and representative of *n* = 10 patients (two biological replications). P values were calculated using a one-sample *t* test compared with 0 (A) or a paired two-tailed Student's *t* test (B). *, P < 0.05; **, P < 0.01. ns, not significant.

and was also downregulated in dermal myofibroblasts (Fig. 5 A, arrows, red). Moreover, we also examined CFIm25 levels in skin fibrosis in a second dermal fibrosis model, the tight skin 1 (TSK1) mouse model. In this model, spontaneous skin fibrosis results from a tandem duplication within the fibrillin-1 gene (Siracusa et al., 1996). A similar CFIm25 downregulation was observed in the skin of TSK1 mice (Figs. 5 C and S3 B). Overall, our data suggest that CFIm25 downregulation is a common feature in human SSc and murine dermal fibrosis.

KO of *CFIm25* in fibroblasts exaggerates dermal fibrosis
Based on the finding that *CFIm25* KD promotes activation of the TGFβ pathway and COL(I) synthesis, we further investigated whether *CFIm25* depletion in vivo affects bleomycin-induced skin fibrosis. We generated homozygous Col1a1-creER^T2-*CFIm25*^f/f mice to conditional KO *CFIm25* expression in Col1a1 expression cells, including fibroblasts. 6-wk-old Col1a1-creER^T2-*CFIm25*^f/f and control Col1a1-creER^T2 mice were injected with tamoxifen for 5 d to induce Cre activation. As shown in Figs. 6 A

and S4 A, Cre was successfully expressed in dermal fibroblasts of Col1a1-creER^T2-*CFIm25*^f/f and control Col1a1-creER^T2 mice, and CFIm25 expression was dramatically suppressed in Col1a1-creER^T2-*CFIm25*^f/f fibroblasts. Of note, although the used promoter in this strain (2.3-kb proximal Col1a1) has been shown to be active in osteoblasts and odontoblasts (Kim et al., 2004; Rossert et al., 1995; Slack et al., 1991), we did not observe any dental or bone abnormalities 4 wk after Cre-activation (data not shown), possibly due to the fact that the Cre-activation occurred in adult mice. 1 wk after the last tamoxifen injection, mice were treated with repeated s.c. bleomycin to induce skin fibrosis. COL(I) protein levels (Figs. 6 B and S4 B), as well as dermal thickness (Fig. 6, C and D), were increased in bleomycin-treated mice, suggesting dermal fibrosis was successfully induced in our model. Notably, CFIm25 protein expression was slightly decreased in the skin of PBS-treated Col1a1-creER^T2-*CFIm25*^f/f mice compared with controls, and it was further downregulated in the conditional KO mice treated with bleomycin, possibly due to the activation and amplification of fibroblasts upon bleomycin
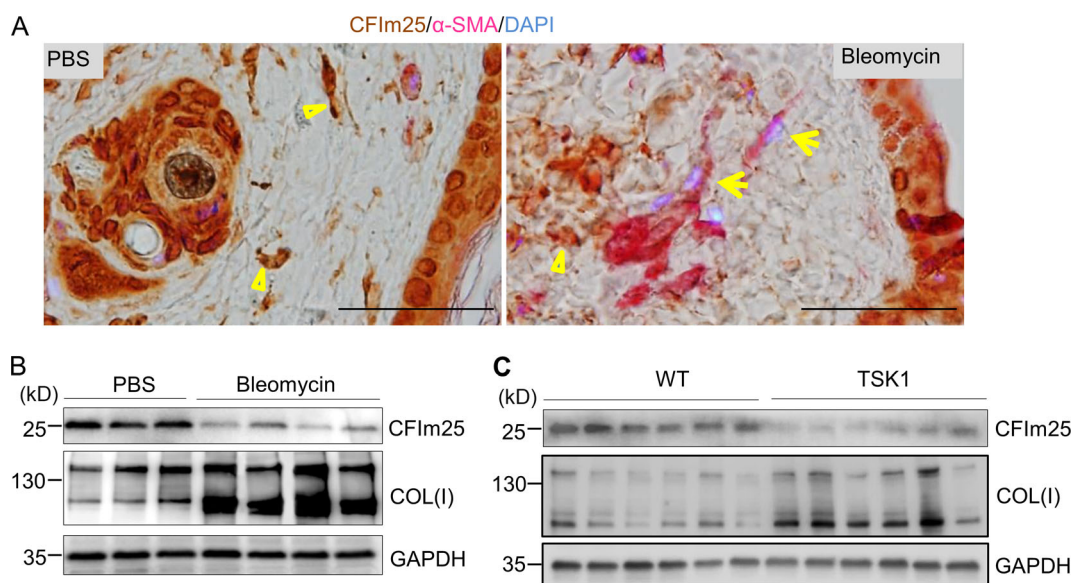
Figure 5. **CFIm25 is decreased in murine dermal fibrosis. (A)** Immunohistochemistry showing CFIm25 (brown) and α-SMA (red) staining in the skin of mice subcutaneously treated with PBS or bleomycin (*n* = 10). Arrowheads show CFIm25+ cells, and arrows point to α-SMA+ myofibroblasts. Scale bars = 25 µm. **(B and C)** CFIm25 protein expression was determined in the skin lysate from (B) mice injected with PBS or bleomycin; and (C) 8- to 10-wk-old WT and TSK1 mice. COL(I) was used as a marker for fibrosis.
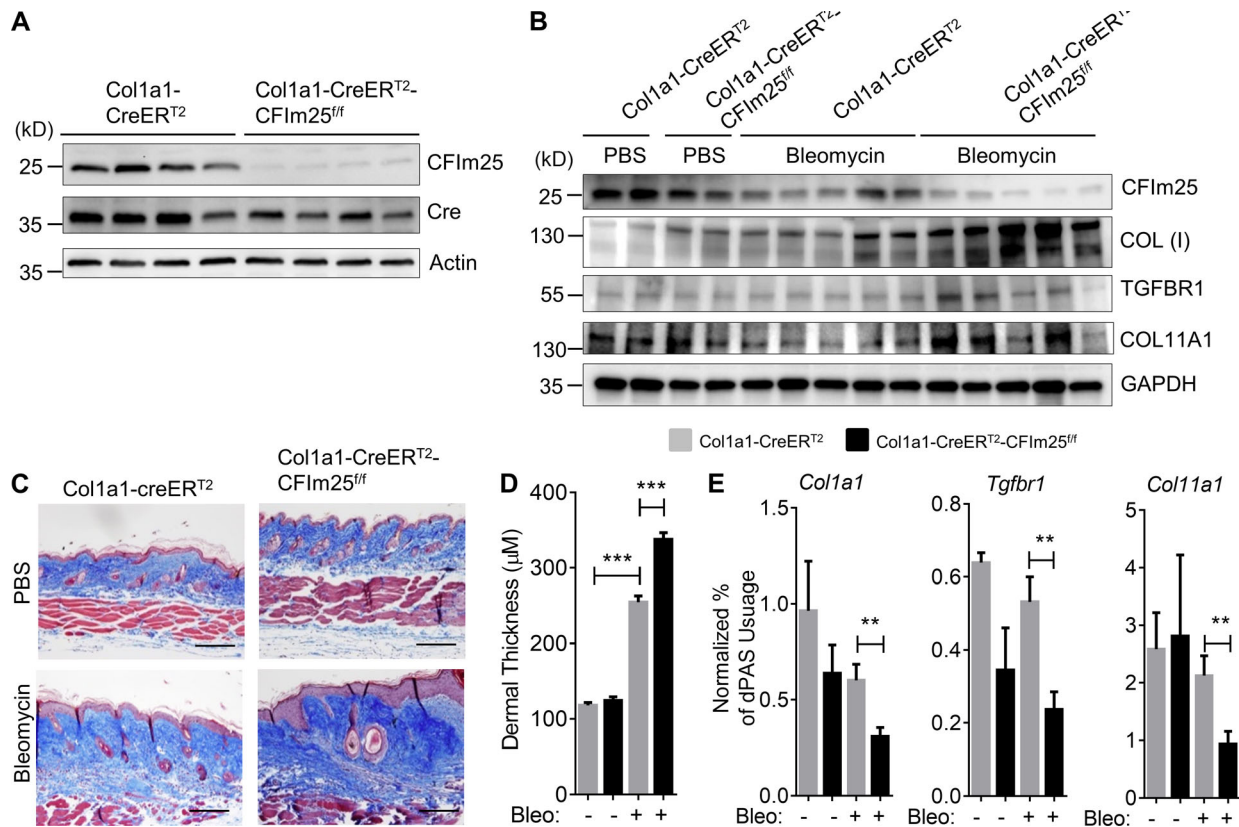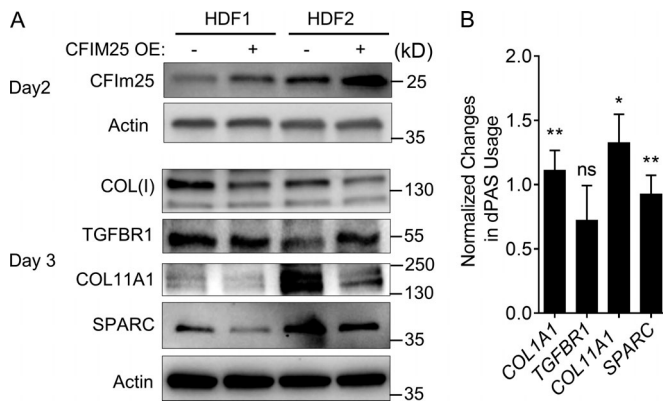
Figure 6. **Knocking out *CFIm25* in fibroblasts promotes dermal fibrosis and APA.** 6- to 8-wk-old Col1a1-creER[T2] and Col1a1-creER[T2]-*CFIm25*[f/f] mice were treated with tamoxifen for 5 d to induce Cre activation. **(A)** Western blot shows Cre expression and a downregulation of *CFIm25* in primary fibroblasts isolated from Col1a1-creER[T2]-*CFIm25*[f/f] mice (n = 4). Tamoxifen-treated mice were then administrated with s.c. PBS/bleomycin 6 d a week for 4 wk (n = 10). **(B)** Western blot was performed to confirm the downregulation of CFIm25 and the upregulation of fibrotic makers in skin of PBS/bleomycin-treated Col1a1-creER[T2] and Col1a1-creER[T2]-*CFIm25*[f/f] mice. **(C)** Masson's trichrome showing dermal fibrosis in different treatment groups; the data are quantitated in D. Scale bars = 125 μm. **(E)** The dPAS usage for *Col1a1, Tgfbr1,* and *Col11a1* was determined using RT-qPCR. Data are mean ± SEM and were analyzed using one-way ANOVA followed by a Sidak's multiple comparisons test (D) or unpaired two-tailed Student's *t* test (E). n = 2 independent experiments (six to eight mice per group, two biological replications). **, P < 0.01; ***, P < 0.001.

treatment (Fig. 6 B). Interestingly, COL(I) expression was already increased in the Col1a1-creER[T2]-*CFIm25*[f/f] mice without bleomycin treatment, and it was further increased in the Col1a1-creER[T2]-*CFIm25*[f/f] mice upon treatment with bleomycin (Fig. 6 B). Although TGFBR1 and COL11A1 protein levels did not differ in the PBS group between the knockout and control mice, they were enhanced in *CFIm25* depleted mice in the bleomycin group (Figs. 6 B and S4 B). In parallel, dermal thickness was also further increased in *CFIm25* KO mice treated with bleomycin (Fig. 6, C and D), indicating that depletion of *CFIm25* in fibroblasts potentiates bleomycin-induced dermal fibrosis. We have previously shown that *Col1a1, Tgfbr1,* and *Col11a1* are directly targeted by *CFIm25* in HDFs and show 3′UTR shortening in SSc skin. To understand whether similar mechanisms are involved in mice, we checked the dPAS usage of these three genes and found all three genes had 3′UTR shortening in the skin of Col1a1-creER[T2]-*CFIm25*[f/f] mice treated with bleomycin (Fig. 6 E). Of note, we could not investigate the dPAS usage in SPARC, the other above-investigated key profibrotic transcript, because SPARC lacks the annotation to APA in mice. Cumulatively, these data suggest that *CFIm25* depletion in

fibroblasts potentiates dermal fibrosis by regulating the APA of profibrotic factors/ECMs and enhancing their translation.

CFIm25 OE attenuates fibrotic protein expression in skin fibroblasts

To understand whether the fibrotic phenotype of *CFIm25* KD can be reversed by *CFIm25* OE, we constructed a *CFIm25* OE lentivirus using the pLV-EF1a-IRES-Puro Vector that contains a human elongation factor-1 α (EF-1a) promoter upstream of an internal ribosome entry site (IRES) element to coexpress puromycin marker. The human *CFIm25* coding domain sequence (CDS) was placed between the EF-1a and IRES. The IRES allows the expression of CFIm25 and puromycin marker from a single mRNA, thus ensuring the coexpression of CFIm25 and puromycin marker in the same cells. A successful CFIm25 OE (Fig. 7 A) and 3′UTR lengthening of *CFIm25* target genes *COL1A1, TGFBR1, COL11A1,* and *SPARC* (Fig. 7 B) were detected in skin fibroblasts infected with *CFIm25* OE lentivirus. Consistent with 3′UTR lengthening, the protein levels of COL1A1, COL11A1, and SPARC were decreased 3 d after *CFIm25* OE in skin fibroblasts (Fig. 7 A). Overall, our data indicate that fibrotic protein

Weng et al.
CFIm25 mediated APA in dermal fibrosis

Journal of Experimental Medicine
https://doi.org/10.1084/jem.20181384

6

Figure 7. **CFIm25 OE lentivirus promotes 3′UTR lengthening and inhibits protein translation of profibrotic factor and ECMs in skin fibroblasts.** Two HDFs were infected with control or *CFIm25*-overexpressing lentivirus at 25 MOI. **(A)** Western blots were performed to determine *CFIm25* OE 2 d after lentivirus infection, and the expression of COL(I), TGFBR1, COL11A1 and SPARC 3 d after lentivirus infection. **(B)** The dPAS usage of *COL1A1*, *TGFBR1*, *COL11A1*, and *SPARC* were determined in HDFs infected with lentivirus for 3 d. Data are presented as mean $\log_2$ (percentage of long transcript in *CFIm25*-overexpressing cells/percentage of long transcript in control cells) ± SEM; n = 3 independent experiments (two cell lines, two biological replications). P value was determined using a one-sample *t* test versus 0. *, P < 0.05; **, P < 0.01.

expression can be suppressed by augmenting the expression of *CFIm25*.

CFIm25 OE attenuates bleomycin-induced skin fibrosis

To further investigate the ability of *CFIm25* OE to impact APA and skin fibrosis in mice, 6-wk-old female C57BL6 mice were injected with GFP or CFIm25-IERS-GFP OE lentivirus s.c. 1 wk before, 1 wk after, and 3 wk after the initial s.c. bleomycin injection. *CFIm25* OE lentivirus significantly increased dermal *CFIm25* transcript and protein levels (Figs. 8 A and S5 B) and inhibited the expression of COL(I), fibronectin, TGFBR1, COL11A1, and SPARC (Figs. 8 A and S5 C). dPAS analysis demonstrated that *Col1a1, Tgfbr1,* and *Col11a1* underwent 3′UTR lengthening (Fig. 8 B). Although *Sparc* had no APA in *CFIm25* overexpressing skin, its protein levels were decreased possibly due to an indirect regulation. In parallel with these findings, the pepsin-soluble collagen levels (Fig. 8 C), skin thickness (Fig. 8, D and E), number of α-SMA positive cells (Fig. 8 F), and picrosirius red–stained area (Fig. 8 G) were significantly reduced in skin infected with *CFIm25* OE lentivirus. Taken together, these data suggest that *CFIm25* OE attenuates bleomycin-induced skin fibrosis in mice.

Discussion

The present study evaluated the role of *CFIm25* as an important APA regulator in skin fibrosis. Our data demonstrate a consistent downregulation of *CFIm25* in skin samples collected from SSc patients, and this downregulation was mainly detected in (myo)fibroblasts. RNA-seq detected significant APA events in human skin fibroblasts upon *CFIm25* KD and identified important fibrotic TGFβ-regulated genes targeted by *CFIm25*.

Moreover, we demonstrated that key verified *CFIm25*-targeted fibrotic genes have shortened 3′UTRs in affected SSc skin. Similar *CFIm25* downregulation was also observed in mouse models of skin fibrosis. Lastly, transgenic mice with *CFIm25* depletion in fibroblasts had exaggerated skin fibrosis, while *CFIm25* restoration attenuated skin fibrosis in mouse. Taken together, our findings characterized a previously unknown importance of CFIm25 in skin fibrosis and link a novel role of APA to SSc pathogenesis.

To our knowledge, this is the first study to link APA and its key regulator, CFIm25, to dermal fibrosis. The role of APA as a RNA regulation process has been reported in various human physiological conditions and diseases. Transcripts with longer 3′UTRs were observed during embryonic development (Ji et al., 2009) and neuron differentiation (Shepard et al., 2011), as well as the development of the central nervous system (Hilgers et al., 2011; Smibert et al., 2012). Several recent studies have shown that global 3′UTR shortening is present in malignancies (Xia et al., 2014; Xiang et al., 2018) and is associated with poorer prognosis in breast and lung cancers (Lembo et al., 2012). Disease-specific APA signatures in numerous genes are also identified in cardiac disorders (Creemers et al., 2016). APA also contributes to key immunological responses, including B cell differentiation (Takagaki et al., 1996) and T cell activation (Chuvpilo et al., 1999), as well as lipopolysaccharide-stimulated macrophages (Shell et al., 2005). In addition, APA plays an important role in cellular processes, including cell proliferation (Elkon et al., 2012; Sandberg et al., 2008; PLOS Genetics Staff, 2016), cell fate determination (Brumbaugh et al., 2018; Ji and Tian, 2009), and cell senescence (Han et al., 2015 Preprint). In the current study, we observed that *CFIm25*, an important APA regulator, was downregulated in SSc skin, as well as in murine dermal fibrosis models. Moreover, several key fibrotic genes, including *COL1A1* (Jimenez and Saitta, 1999), *COL11A1*, *TGFBR1*, and *SPARC*, showed significant 3′UTR shortening in affected SSc skin. These four genes had increased transcript levels in our previous SSc skin gene expression study and have been implicated in SSc pathogenesis (Jimenez and Saitta, 1999; Lafyatis, 2014; Zhou et al., 2006). Cumulatively, our findings uncovered APA as a novel amplification mechanism for the exaggerated dermal fibrosis in SSc.

Important functions for *CFIm25* through regulating APA have been reported in several cellular processes. *CFIm25* depletion promoted neurite outgrowth (Fukumitsu et al., 2012), enhancing cancer cell proliferation through upregulating oncogenes (Chu et al., 2019; Masamha et al., 2014; Sun et al., 2017), inhibiting cancer cell apoptosis (Zhu et al., 2016), increasing hepatocellular carcinoma metastasis (Wang et al., 2018), controlling *Entamoeba histolytica* parasite (Ospina-Villa et al., 2017), and facilitating the generation of induced pluripotent stem cells and impairing the differentiation of myeloid precursors and embryonic stem cells (Brumbaugh et al., 2018). In the present study, *CFIm25* expression was downregulated in fibrotic skin, and this downregulation was mainly observed in (myo)fibroblasts, the key cells producing excessive ECM in skin fibrosis, suggesting that *CFIm25* and APA are linked to the pathogenesis of skin fibrosis. Indeed, skin fibroblasts with *CFIm25* KD have increased collagen
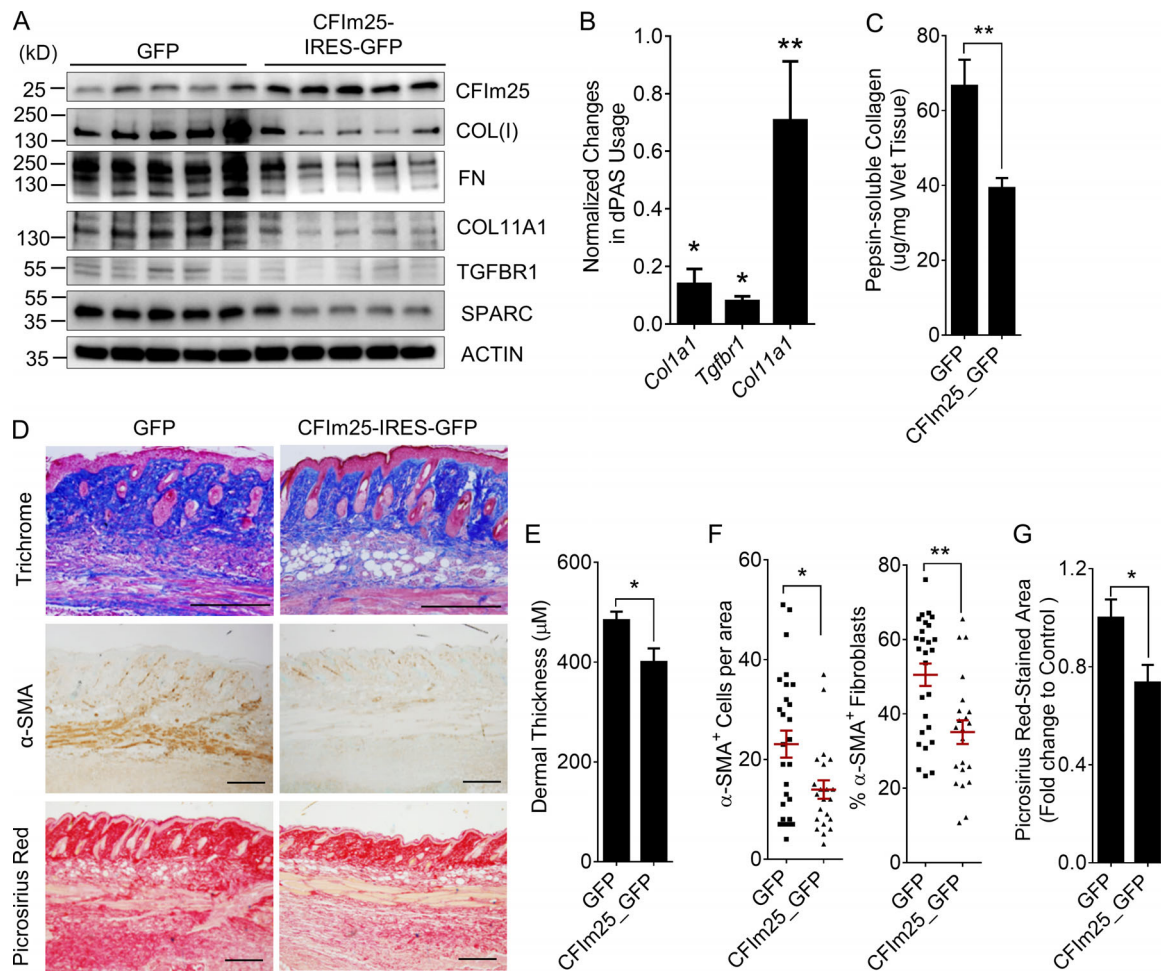
Figure 8. **CFIm25 OE prevents bleomycin-induced skin fibrosis.** 6-wk-old mice were injected with s.c. GFP or CFIm25-IRES-GFP–overexpressing lentivirus (10×10^7 PFU/ml, 50 µl per spot) 1 wk before, 1 wk after, and 3 wk after the first bleomycin injection, and mice were injected with repeated s.c. bleomycin six times a week for 4 wk. Skin was collected 28 d after the first bleomycin injection for analysis. **(A)** Western blot was performed to determine the expression of CFIm25, COL(I), fibronectin (FN), TGFBR1, COL11A1, and SPARC. **(B)** The dPAS usage of *Col1a1*, *Tgfbr1*, and *Col11a1* was determined. Data are presented as $\log_2$ (percentage of long transcript in *CFIm25*-overexpressing skin/percentage of long transcript in control skin). **(C)** Sircol assay was performed to determine the pepsin-soluble collage levels in skin. **(D)** Masson's trichrome, α-SMA, and picrosirius red staining showing dermal fibrosis in different treatment groups. Scale bars =125 µm. **(E)** Histological dermal thickness. **(F)** The numbers of α-SMA⁺ fibroblasts per field (left panel) as well as the percentage of α-SMA⁺ fibroblasts over the total fibroblasts (right panel). **(G)** The percentage of picrosirius red–stained area was measured, and data are presented as fold change to GFP control. Data are mean ± SEM of $n = 2$ independent experiments (five mice per group; C, D, F, and G) with two biological replications (B). P value was determined using one sample *t* test (B) or unpaired two-tailed Student's *t* test (C, D, F, and G). *, P < 0.05; **, P < 0.01.

production and enhanced key fibrotic protein expression. Consistent with our overall hypothesis, *CFIm25* depletion in murine dermal fibroblasts led to exaggerated skin fibrosis upon s.c. bleomycin administration. Moreover, OE of *CFIm25* promoted the 3′UTR lengthening of fibrotic markers and inhibited their expression and eventually attenuated skin fibrosis. In summary, our findings indicate a novel function of *CFIm25* in the pathogenesis of skin fibrosis.

CFIm25-mediated suppression of gene expression is mainly performed through a widespread distal-to-proximal switch of PASs (Brumbaugh et al., 2018; Kubo et al., 2006; Masamha et al., 2014). Consistent with findings in other cell types (Brumbaugh et al., 2018; Masamha et al., 2014; Sun et al., 2017), we demonstrated for the first time using a global, unbiased RNA-seq approach that *CFIm25* KD in dermal fibroblasts leads to 3′UTR shortening in 971 transcripts and 3′UTR lengthening in only 93

transcripts. The shortened transcripts can be more stable as they evade 3′UTR-regulating factors, including miRNAs, and hence enhancing their protein translation. Indeed, we verified that *COL1A1*, *CO11A1*, *TGFBR1*, and *SPARC*, four fibrotic genes involved in the TGFβ pathway, had 3′UTR shortening and elevated protein expression upon *CFIm25* KD. The other function of 3′UTR shortening of target genes could be releasing miRNAs and RNA-binding proteins that would have been bound to the longer form, thus resulting in the redistribution of RNA-binding proteins and miRNA (Park et al., 2018). However, it should be noted that 3′UTR shortening does not lead to increased protein translation in all genes (Brumbaugh et al., 2018). The missing correlation between 3′UTR shortening and protein abundance in some genes could depend on the availability of miRNAs and RNA regulatory factors in various cells. That also explains why *CFIm25* depletion has a different impact on various cells,

including cancer cells, stem cells, immune cells, and skin fibroblasts. In the present study, we focused on dermal fibroblasts, the key cell type for the observed exaggerated ECM deposition in SSc skin.

An unbiased, global Ingenuity Pathway Analysis (IPA) predicted TGFβ1 as the top upstream regulator of the 971 genes that showed 3′UTR shortening upon *CFIm25* depletion. Specifically, 97 out of these 971 (~10%) *CFIm25*-targeted genes can be regulated by TGFβ1, including key fibrotic genes known to play a role in SSc pathogenesis such as collagens, integrins (Ray, 2013), TGFBR1 (Pannu et al., 2007), and SPARC (Bhattacharyya et al., 2011; Lafyatis, 2014; Zhou et al., 2006). Consistent with this prediction, TGFβ1 was the top predicted regulator for SSc skin gene expression signature in our previous global gene expression studies (Assassi et al., 2015). Moreover, our skin immunostaining experiments indicated that CFIm25 is specifically downregulated in (myo)fibroblasts of patients with SSc, a cell type prominently targeted by TGFβ1, suggesting that *CFIm25* depletion might function as an enhancing mediator of TGFβ1 response in SSc dermal fibroblasts. TGFβ1 is a master regulator of fibrotic diseases that drives fibroblast proliferation, myofibroblast differentiation, and ECM synthesis (Lafyatis, 2014). TGFβ1 mainly functions through TGFBR1 and TGFBR2 to activate receptor signaling (Meng et al., 2016). We found *TGFBR1*, as well as TGFβ1 target genes *COL1A1*, *COL11A1*, and *SPARC*, had 3′UTR shortening and enhanced protein expression in *CFIm25*-depleted fibroblasts, suggesting that *CFIm25* depletion is sufficient to activate TGFβ1 signaling. Consistent with this notion, *CFIm25* depletion in fibroblasts in a bleomycin-induced murine dermal fibrosis model led to 3′UTR shortening of the same key TGFβ1-regulated genes (*Col1a1*, *Tgfbr1*, and *Col11a1*) and enhanced their protein expression and resulted ultimately in increased fibrotic response. In summary, our data suggest that TGFβ1 is an upstream regulator of the *CFIm25* depletion signature, and downregulation of *CFIm25* in turn promotes TGFβ1 signaling and enhances skin fibrosis.

Although our data indicate that TGFβ1 is a key upstream regulator of the *CFIm25* depletion signature, future studies are needed to examine the mechanistic link between TGFβ1 and *CFIm25* depletion. Moreover, considering the diverse function of *CFIm25* in different cell types, it will be instructive to elucidate the role of *CFIm25* in other type of cells, such as immune cells, involved in SSc pathogenesis. In addition to *CFIm25* studied here, there are other proteins that can also modulate APA. For example, two other components of the CFIm complex, CFIm59 and CFIm68, also promote the usage of dPAS sites, and depletion of CFIm68 causes widespread distal-to-proximal PAS shifting (Martin et al., 2012; Masamha et al., 2014). Although our study demonstrates for the first time an important role for APA in SSc pathogenesis focusing on *CFIm25* mediating 3′UTR shortening, it may prove useful to investigate the role of other APA regulators in fibrosis and SSc pathogenesis in future studies.

SSc is an enigmatic disease with no US Food and Drug Administration–approved medications and the highest mortality rate among major rheumatic diseases. Herein, we link for the first time a recently discovered key regulator of RNA processing to the exaggerated dermal fibrosis in SSc. Specifically, the downregulation of the RNA-processing factor *CFIm25* leads to 3′UTR shortening of key TGFβ-regulated profibrotic genes and exaggerated skin fibrosis. Methods aimed at *CFIm25* rescue can be a potential therapeutic target in this devastating fibrotic disease.

Materials and methods

Human samples

Skin biopsy samples were collected from the Genetic versus Environment In Scleroderma Outcome Study cohort at the University of Texas Health Science Center at Houston and age-, gender-, and ethnicity matched controls. All patients fulfilled the 2012 American College of Rheumatology/European League Against Rheumatism Classification Criteria (van den Hoogen et al., 2013) and had diffuse cutaneous involvement, disease duration <3.5 yr at enrollment, and affected skin at the site of skin biopsy. The healthy control subjects had no personal or family medical history of autoimmune diseases. Biopsy samples (3-mm punch) were obtained from the ulnar, dorsal aspect of the forearm around the proximal one-third junction. All subjects provided written informed consent, and the study was approved by the institutional review boards at the University of Texas Health Science Center.

Mice

Mice were housed in pathogen-free conditions at the University of Texas Health McGovern Medical School, Houston, TX. All experiments were approved by the University of Texas Health Animal Welfare Committee. All mice were on the C57BL/6J background. WT, Col1a1-Cre (B6.Cg-Tg(Col1a1-cre/ERT2)1Crm/J), and TSK1 mice were purchased from Jackson Laboratory. *CFIm25*[f/f] mice were generated using floxed alleles designed to delete exons 2 and 3 of the *CFIm25* gene (*CFIm25*[f/f]; Ozgene). To induce Cre recombination to knockout *CFIm25* specifically in fibroblasts, 6-wk-old transgenic mice (*CFIm25*[f/f] Col1a1-Cre) or age- and gender-matched littermate controls (Col1a1-cre) were i.p. injected with 75 mg/kg/d tamoxifen for 5 d (Eckle et al., 2013; Perl et al., 2002). To induce skin fibrosis, the mice were administrated with repeated s.c. bleomycin (0.02 U/mice/d, injected six times a week for 4 wk). The first injection of bleomycin was administered 7 d after the end of tamoxifen treatment.

Immunohistochemistry and immunofluorescence

Mouse or human skin was dehydrated, paraffin embedded, and sectioned (4 µm). Sections were rehydrated, quenched with 3% hydrogen peroxide, incubated in citric buffer (VectorLabs) for antigen retrieval, and blocked with Avidin/Biotin Blocking System (VectorLabs) and then 5% normal goat serum.

For double immunohistochemistry staining for CFIm25 and α-SMA, sections were incubated with antibodies for CFIm25 (1:400; Proteintech) overnight at 4°C and then with biotinylated anti-Rabbit antibodies (1:1,000; VectorLabs) for 1 h at room temperature and ABC Elite streptavidin reagents for 30 min at room temperature. Slides were then developed with 3,3-diaminobenzidine (Sigma-Aldrich). After development, the slides

Weng et al.
CFIm25 mediated APA in dermal fibrosis

Journal of Experimental Medicine
https://doi.org/10.1084/jem.20181384

9

were incubated with mouse anti-α-SMA antibodies (1:1,000; Sigma-Aldrich) overnight at 4°C, anti-mouse secondary antibodies (1:1,000; VectorLabs) and alkaline phosphatase ABC Elite streptavidin reagents and developed using Vector Red Substrate (VectorLabs).

For CFIm25/α-SMA immunofluorescence dual staining, skin sections were first stained with CFIm25 and developed with Vecto Red Substrate. The sections were then blocked with normal horse serum and incubated with anti-α-SMA antibodies and Alexa Fluor 488 Goat Anti-Mouse IgG (Life Technologies). Slides were finally mounted with ProLong Gold Antifade Mountant with DAPI (Life Technologies).

Masson's trichrome and picrosirius red staining
Paraffin-embedded skin slides were rehydrated and stained with Masson's trichrome (Sigma-Aldrich) or picrosirius red kit (Abcam). The thickness of the dermis, defined as the distance between the epidermal-dermal junction to the dermal-adipose layer junction, was measured blindly at six randomly selected sites/microscopic fields in each skin sample (Wu et al., 2012). The picrosirius red–stained skin was quantified using ImageJ and macro language (available at https://imagej.nih.gov/ij/docs/examples/stained-sections/index.html). The percentage of positive picrosirius red–stained area was determined, and data were normalized to the GFP control.

Cell culture and transfection
Primary human skin fibroblasts were isolated using an outgrowth model from skin punch from normal donor and SSc patients. Isolated fibroblasts were treated in DMEM (Sigma-Aldrich) containing 10% fetal bovine serum and 1% antibiotics to avoid contamination, and mycoplasma infection was tested using the MycoAlert Mycoplasma Detection Kit (Lonza). Cell culture was maintained at 37°C in a humidified 5% carbon dioxide atmosphere.

To knock down *CFIm25*, fibroblasts were transfected with 50 ng/ml *CFIm25* or control siRNA (Sigma-Aldrich) using Lipofectamine RNAiMAX (ThermoFisher Scientific) on day 0 and day 1, and RNA and protein were collected on day 4 for analysis.

RT-qPCR
Total RNA was extracted using RNeasy Mini Kit (Qiagen) and reverse-transcribed using iScript Reverse Transcription Supermix (Bio-Rad). Real-time PCR was performed under Lightcycler 96 (Roche), and data were quantified using the comparative Ct method and presented as mean ratio to β-actin or 18s rRNA.

The APA of target genes was determined using a previously described PCR-based method (Masamha et al., 2014). For each candidate gene, two pairs of primers were designed with one targeting the open reading frame to represent the total transcript level and the other targeting sequences just before the dPAS to detect long transcripts that used the dPAS (Fig. 3 B). Percentage of dPAS usage was calculated as $\Delta CT = CT_{distal} - CT_{total}$. Data were presented as fold changes normalized to control by calculating $\Delta\Delta CT = \Delta CT_{average\ target} - \Delta CT_{average\ of\ control}$. A negative $\Delta\Delta CT$ value indicates the mRNA has 3′UTR shortening compared with controls, and this approach has been used to

quantify APA (Masamha et al., 2014). The primers used for this study are listed in Table S3.

RNA-seq and data analysis
Total RNA-seq was performed by HiSeq 2000 (Novogene) using the poly(A) enrichment method. This allowed us to obtain a precise and complete snapshot of the transcriptome and enabled the identification of transcript expression as well as APA. Paired-end RNA-seq was performed to yield a minimum of 80 million reads per sample. Raw sequence data have been deposited in the Gene Expression Omnibus database (accession no. GSE137276). RNA-seq gene expressions were quantified by RSEM. To identify genes undergoing APA upon *CFIm25* depletion, a well-established algorithm DaPars (https://github.com/ZhengXia/DaPars; Xia et al., 2014) was used to predict the proximal APA site and estimate the abundance of long and short forms of 3′UTRs, and then the percentage of distal polyadenylation site usage index (PDUI) was calculated for each transcript. Briefly, DaPars uses a linear regression model to predict the proximal APA site and estimates the abundance of long-form and short-form 3′UTRs and then calculates the PDUI. For the comparison between si_RNA- and si_*CFIm25*–transfected fibroblasts, genes with a difference of PDUI ≥0.15 in at least three HDFs were considered to have APA.

To identify upstream regulator cytokines/growth factors, the list of genes with significant 3′UTR shortening upon *CFIm25* depletion was uploaded into IPA. The goal of Upstream Regulator Analysis in IPA is to identify upstream regulators of any given dataset and predict whether they are activated or inhibited given the observed gene expression changes. This analysis utilizes a Z score algorithm to make predictions. The Z score algorithm is designed to reduce the chance that random data will generate significant predictions. Upstream Regulator Analysis is derived from expected causal effects between upstream regulators and targets; the expected causal effects are based on the literature compiled and updated on a regular basis in the Ingenuity Knowledge Base.

CFIm25 OE lentivirus construction and cell treatment
CFIm25 OE lentivirus vector was generated by cloning the CDS of human *CFIm25* into the pLV-EF1a-IRES-Puro Vector (Addgene) that contains an EF-1a promoter upstream of an IRES element to coexpress puromycin marker. *CFIm25* CDS were inserted between the EF-1a and IRES. The IRES allows the expression of CFIm25 and puromycin marker from a single mRNA, thus ensuring the coexpression of CFIm25 and puromycin marker in the same cells. The empty vector without any insertion was used as control. The *CFIm25*-overexpressing and control lentiviruses were then generated using the third-generation Lentivirus Packing System (Abm). The lentivirus titer was determined using the qPCR Lentivirus Titration (Titer) Kit (Abm). Human skin fibroblasts were transfected with *CFIm25* OE or control virus at a multiplicity of infection (MOI) of 25.

CFIm25 OE in murine model of skin fibrosis
Another CFIm25-overexpressing lentivirus vector, pCMV-CFIm25-IRES-GFP, was generated by inserting the CFIm25 CDS

Weng et al.
CFIm25 mediated APA in dermal fibrosis

Journal of Experimental Medicine   10
https://doi.org/10.1084/jem.20181384

into the PCIG3 (pCMV-IRES-GFP; Addgene) vector. PCIG3 vector without any insertion was used as control. These vectors replaced the puromycin gene with GFP gene, allowing us to track CFIm25 expression in vivo. Lentiviruses were generated using the second-generation lentivirus packing system (Addgene) to achieve higher titer. 6-wk-old female C57BL6 mice were s.c. injected with *CFIm25* OE or control lentivirus (50 µl 10 × 10^7 PFU/ml at each spot) 1 wk before, 1 wk after, and 3 wk after initial bleomycin injection. Then, mice were injected with repeated s.c. bleomycin (0.02 U/mice/d, injected six times a week for 4 wk) starting 1 wk after the first lentivirus injection. Skin samples were collected on day 28 after the first bleomycin injection for analysis.

Sircol collagen assay
Fresh collected mouse skin were weighted and homogenized in 0.5 M acetic acid. For each milligram of mouse skin, 0.1 mg pepsin (Sigma-Aldrich) was added. Skin samples were rocked overnight at room temperature to release collagen. Digested skin samples were centrifuged and the supernatant was collected to determine the collagen concentration using the Sircol Soluble Collagen Assay kit (Biocolor). The final data were normalized to the wet skin weight.

Statistics
Results are expressed as the mean ± SEM. Data were analyzed using the Student's *t* test for comparison of two groups or ANOVA (GraphPad Software). The number of asterisks represents the degree of significance with respect to P value. P values < 0.05 were considered significant.

Online supplemental material
Fig. S1 shows the number and percentage of CFIm25 and α-SMA stained cells in control and SSc skin, as well as the densitometry of Western blot showing CFIm25 and COL(I) expression in control and SSc skin. Fig. S2 shows the densitometry analysis of the protein expression of fibrotic factors in normal HDFs with CFIm25 depletion. Fig. S3 shows the densitometry analysis of CFIm25 and COL(I) protein expression in murine models of dermal fibrosis. Fig. S4 shows the densitometry analysis of CFIm25 and fibrotic marker expression in the mouse skin samples with CFIm25 knockout. Fig. S5 shows the densitometry analysis of CFIm25 and its targets expression in fibroblasts and mouse skin samples with CFIm25 OE. Table S1 shows demographic and clinical characteristics of participants in the immunohistochemistry experiments. Table S2 shows demographic and clinical characteristics of participants in the dPAS experiments. Table S3 shows the primers used for RT-qPCR.

Acknowledgments

References

Assassi, S., W.R. Swindell, M. Wu, F.D. Tan, D. Khanna, D.E. Furst, D.P. Tashkin, R.R. Jahan-Tigh, M.D. Mayes, J.E. Gudjonsson, and J.T. Chang. 2015. Dissecting the heterogeneity of skin gene expression patterns in systemic sclerosis. *Arthritis Rheumatol.* 67:3016–3026. https://doi.org/10.1002/art.39289

Bhattacharyya, S., J. Wei, and J. Varga. 2011. Understanding fibrosis in systemic sclerosis: shifting paradigms, emerging opportunities. *Nat. Rev. Rheumatol.* 8:42–54. https://doi.org/10.1038/nrrheum.2011.149

Brumbaugh, J., B. Di Stefano, X. Wang, M. Borkent, E. Forouzmand, K.J. Clowers, F. Ji, B.A. Schwarz, M. Kalocsay, S.J. Elledge, et al. 2018. Nudt21 Controls Cell Fate by Connecting Alternative Polyadenylation to Chromatin Signaling. *Cell.* 172:629–631. https://doi.org/10.1016/j.cell.2017.12.035

Chu, Y., N. Elrod, C. Wang, L. Li, T. Chen, A. Routh, Z. Xia, W. Li, E.J. Wagner, and P. Ji. 2019. Nudt21 regulates the alternative polyadenylation of Pak1 and is predictive in the prognosis of glioblastoma patients. *Oncogene.* 38:4154–4168. https://doi.org/10.1038/s41388-019-0714-9

Chuvpilo, S., M. Zimmer, A. Kerstan, J. Glöckner, A. Avots, C. Escher, C. Fischer, I. Inashkina, E. Jankevics, F. Berberich-Siebelt, et al. 1999. Alternative polyadenylation events contribute to the induction of NF-ATc in effector T cells. *Immunity.* 10:261–269. https://doi.org/10.1016/S1074-7613(00)80026-6

Creemers, E.E., A. Bawazeer, A.P. Ugalde, H.W. van Deutekom, I. van der Made, N.E. de Groot, M.E. Adriaens, S.A. Cook, C.R. Bezzina, N. Hubner, et al. 2016. Genome-Wide Polyadenylation Maps Reveal Dynamic mRNA 3′-End Formation in the Failing Human Heart. *Circ. Res.* 118:433–438. https://doi.org/10.1161/CIRCRESAHA.115.307082

Curinha, A., S. Oliveira Braz, I. Pereira-Castro, A. Cruz, and A. Moreira. 2014. Implications of polyadenylation in health and disease. *Nucleus.* 5:508–519. https://doi.org/10.4161/nucl.36360

Di Giammartino, D.C., K. Nishida, and J.L. Manley. 2011. Mechanisms and consequences of alternative polyadenylation. *Mol. Cell.* 43:853–866. https://doi.org/10.1016/j.molcel.2011.08.017

Eckle, T., K. Brodsky, M. Bonney, T. Packard, J. Han, C.H. Borchers, T.J. Mariani, D.J. Kominsky, M. Mittelbronn, and H.K. Eltzschig. 2013. HIF1A reduces acute lung injury by optimizing carbohydrate metabolism in the alveolar epithelium. *PLoS Biol.* 11:e1001665. https://doi.org/10.1371/journal.pbio.1001665

Elfving, P., K. Puolakka, H. Kautiainen, L.J. Virta, T. Pohjolainen, and O. Kaipiainen-Seppänen. 2014. Mortality and causes of death among incident cases of systemic lupus erythematosus in Finland 2000-2008. *Lupus.* 23:1430–1434. https://doi.org/10.1177/0961203314543919

Elhai, M., C. Meune, J. Avouac, A. Kahan, and Y. Allanore. 2012. Trends in mortality in patients with systemic sclerosis over 40 years: a systematic review and meta-analysis of cohort studies. *Rheumatology (Oxford).* 51:1017–1026. https://doi.org/10.1093/rheumatology/ker269

Elkon, R., J. Drost, G. van Haaften, M. Jenal, M. Schrier, J.A. Oude Vrielink, and R. Agami. 2012. E2F mediates enhanced alternative polyadenylation in proliferation. *Genome Biol.* 13:R59. https://doi.org/10.1186/gb-2012-13-7-r59

Elkon, R., A.P. Ugalde, and R. Agami. 2013. Alternative cleavage and polyadenylation: extent, regulation and function. *Nat. Rev. Genet.* 14:496–506. https://doi.org/10.1038/nrg3482

Fukumitsu, H., H. Soumiya, and S. Furukawa. 2012. Knockdown of premRNA cleavage factor Im 25 kDa promotes neurite outgrowth. *Biochem. Biophys. Res. Commun.* 425:848–853. https://doi.org/10.1016/j.bbrc.2012.07.164

Gruber, A.R., G. Martin, W. Keller, and M. Zavolan. 2012. Cleavage factor Im is a key regulator of 3′ UTR length. *RNA Biol.* 9:1405–1412. https://doi.org/10.4161/rna.22570

Han, M., G. Lv, H. Nie, T. Shen, Y. Niu, X. Li, M. Chen, X. Zheng, W. Li, C. Ding, et al. 2015. Global lengthening of 3′ untranslated regions of mRNAs by alternative cleavage and polyadenylation in cellular senescence. *bioRxiv.* (Preprint posted December 2, 2015)https://doi.org/10.1101/033480

Hilgers, V., M.W. Perry, D. Hendrix, A. Stark, M. Levine, and B. Haley. 2011. Neural-specific elongation of 3′ UTRs during Drosophila development. *Proc. Natl. Acad. Sci. USA.* 108:15864–15869. https://doi.org/10.1073/pnas.1112672108

Ji, Z., and B. Tian. 2009. Reprogramming of 3′ untranslated regions of mRNAs by alternative polyadenylation in generation of pluripotent stem cells from different cell types. *PLoS One.* 4:e8419. https://doi.org/10.1371/journal.pone.0008419

Ji, Z., J.Y. Lee, Z. Pan, B. Jiang, and B. Tian. 2009. Progressive lengthening of 3′ untranslated regions of mRNAs by alternative polyadenylation during mouse embryonic development. *Proc. Natl. Acad. Sci. USA.* 106:7028–7033. https://doi.org/10.1073/pnas.0900028106

Jimenez, S.A., and B. Saitta. 1999. Alterations in the regulation of expression of the alpha 1(I) collagen gene (COL1A1) in systemic sclerosis (scleroderma). *Springer Semin. Immunopathol.* 21:397–414.

Khanna, D., C.P. Denton, A. Jahreis, J.M. van Laar, T.M. Frech, M.E. Anderson, M. Baron, L. Chung, G. Fierlbeck, S. Lakshminarayanan, et al. 2016. Safety and efficacy of subcutaneous tocilizumab in adults with systemic sclerosis (faSScinate): a phase 2, randomised, controlled trial. *Lancet.* 387:2630–2640. https://doi.org/10.1016/S0140-6736(16)00232-4

Kim, J.E., K. Nakashima, and B. de Crombrugghe. 2004. Transgenic mice expressing a ligand-inducible cre recombinase in osteoblasts and odontoblasts: a new tool to examine physiology and disease of postnatal bone and tooth. *Am. J. Pathol.* 165:1875–1882. https://doi.org/10.1016/S0002-9440(10)63240-3

Kubo, T., T. Wada, Y. Yamaguchi, A. Shimizu, and H. Handa. 2006. Knockdown of 25 kDa subunit of cleavage factor Im in Hela cells alters alternative polyadenylation within 3′-UTRs. *Nucleic Acids Res.* 34:6264–6271. https://doi.org/10.1093/nar/gkl794

Lafyatis, R. 2014. Transforming growth factor β--at the centre of systemic sclerosis. *Nat. Rev. Rheumatol.* 10:706–719. https://doi.org/10.1038/nrrheum.2014.137

Lembo, A., F. Di Cunto, and P. Provero. 2012. Shortening of 3′UTRs correlates with poor prognosis in breast and lung cancer. *PLoS One.* 7:e31129. https://doi.org/10.1371/journal.pone.0031129

Lim, L.P., N.C. Lau, P. Garrett-Engele, A. Grimson, J.M. Schelter, J. Castle, D.P. Bartel, P.S. Linsley, and J.M. Johnson. 2005. Microarray analysis shows that some microRNAs downregulate large numbers of target mRNAs. *Nature.* 433:769–773. https://doi.org/10.1038/nature03315

Linsley, P.S., J. Schelter, J. Burchard, M. Kibukawa, M.M. Martin, S.R. Bartz, J.M. Johnson, J.M. Cummins, C.K. Raymond, H. Dai, et al. 2007. Transcripts targeted by the microRNA-16 family cooperatively regulate cell cycle progression. *Mol. Cell. Biol.* 27:2240–2252. https://doi.org/10.1128/MCB.02005-06

Martin, G., A.R. Gruber, W. Keller, and M. Zavolan. 2012. Genome-wide analysis of pre-mRNA 3′ end processing reveals a decisive role of human cleavage factor I in the regulation of 3′ UTR length. *Cell Reports.* 1:753–763. https://doi.org/10.1016/j.celrep.2012.05.003

Masamha, C.P., Z. Xia, J. Yang, T.R. Albrecht, M. Li, A.B. Shyu, W. Li, and E.J. Wagner. 2014. CFIm25 links alternative polyadenylation to glioblastoma tumour suppression. *Nature.* 510:412–416. https://doi.org/10.1038/nature13261

Maurer, B., N. Graf, B.A. Michel, U. Müller-Ladner, L. Czirják, C.P. Denton, A. Tyndall, C. Metzig, V. Lanius, D. Khanna, and O. Distler. EUSTAR co-authors. 2015. Prediction of worsening of skin fibrosis in patients with diffuse cutaneous systemic sclerosis using the EUSTAR database. *Ann. Rheum. Dis.* 74:1124–1131. https://doi.org/10.1136/annrheumdis-2014-205226

Meng, X.M., D.J. Nikolic-Paterson, and H.Y. Lan. 2016. TGF-β: the master regulator of fibrosis. *Nat. Rev. Nephrol.* 12:325–338. https://doi.org/10.1038/nrneph.2016.48

Ospina-Villa, J.D., N. Guillén, C. Lopez-Camarillo, J. Soto-Sanchez, E. Ramirez-Moreno, R. Garcia-Vazquez, C.A. Castañon-Sanchez, A. Betanzos, and L.A. Marchat. 2017. Silencing the cleavage factor CFIm25 as a new strategy to control Entamoeba histolytica parasite. *J. Microbiol.* 55:783–791. https://doi.org/10.1007/s12275-017-7259-9

Pannu, J., S. Nakerakanti, E. Smith, P. ten Dijke, and M. Trojanowska. 2007. Transforming growth factor-beta receptor type I-dependent fibrogenic gene program is mediated via activation of Smad1 and ERK1/2 pathways. *J. Biol. Chem.* 282:10405–10413. https://doi.org/10.1074/jbc.M611742200

Park, H.J., P. Ji, S. Kim, Z. Xia, B. Rodriguez, L. Li, J. Su, K. Chen, C.P. Masamha, D. Baillat, et al. 2018. 3′ UTR shortening represses tumor-suppressor genes in trans by disrupting ceRNA crosstalk. *Nat. Genet.* 50:783–789. https://doi.org/10.1038/s41588-018-0118-8

Perl, A.K., S.E. Wert, A. Nagy, C.G. Lobe, and J.A. Whitsett. 2002. Early restriction of peripheral and proximal cell lineages during formation of the lung. *Proc. Natl. Acad. Sci. USA.* 99:10482–10487. https://doi.org/10.1073/pnas.152238499

Ray, K. 2013. Connective tissue diseases: Integrins crucial for the onset of fibrosis in systemic sclerosis--a new therapeutic target? *Nat. Rev. Rheumatol.* 9:637. https://doi.org/10.1038/nrrheum.2013.144

Rossert, J., H. Eberspaecher, and B. de Crombrugghe. 1995. Separate cis-acting DNA elements of the mouse pro-alpha 1(I) collagen promoter direct expression of reporter genes to different type I collagen-producing cells in transgenic mice. *J. Cell Biol.* 129:1421–1432. https://doi.org/10.1083/jcb.129.5.1421

Sandberg, R., J.R. Neilson, A. Sarma, P.A. Sharp, and C.B. Burge. 2008. Proliferating cells express mRNAs with shortened 3′ untranslated regions and fewer microRNA target sites. *Science.* 320:1643–1647. https://doi.org/10.1126/science.1155390

Shell, S.A., C. Hesse, S.M. Morris Jr., and C. Milcarek. 2005. Elevated levels of the 64-kDa cleavage stimulatory factor (CstF-64) in lipopolysaccharide-stimulated macrophages influence gene expression and induce alternative poly(A) site selection. *J. Biol. Chem.* 280:39950–39961. https://doi.org/10.1074/jbc.M508948200

Shepard, P.J., E.A. Choi, J. Lu, L.A. Flanagan, K.J. Hertel, and Y. Shi. 2011. Complex and dynamic landscape of RNA polyadenylation revealed by PAS-Seq. *RNA.* 17:761–772. https://doi.org/10.1261/rna.2581711

Singh, P., T.L. Alley, S.M. Wright, S. Kamdar, W. Schott, R.Y. Wilpan, K.D. Mills, and J.H. Graber. 2009. Global changes in processing of mRNA 3′ untranslated regions characterize clinically distinct cancer subtypes. *Cancer Res.* 69:9422–9430. https://doi.org/10.1158/0008-5472.CAN-09-2236

Siracusa, L.D., R. McGrath, Q. Ma, J.J. Moskow, J. Manne, P.J. Christner, A.M. Buchberg, and S.A. Jimenez. 1996. A tandem duplication within the fibrillin 1 gene is associated with the mouse tight skin mutation. *Genome Res.* 6:300–313. https://doi.org/10.1101/gr.6.4.300

Slack, J.L., D.J. Liska, and P. Bornstein. 1991. An upstream regulatory region mediates high-level, tissue-specific expression of the human alpha 1(I) collagen gene in transgenic mice. *Mol. Cell. Biol.* 11:2066–2074. https://doi.org/10.1128/MCB.11.4.2066

Smibert, P., P. Miura, J.O. Westholm, S. Shenker, G. May, M.O. Duff, D. Zhang, B.D. Eads, J. Carlson, J.B. Brown, et al. 2012. Global patterns of tissue-specific alternative polyadenylation in Drosophila. *Cell Reports.* 1:277–289. https://doi.org/10.1016/j.celrep.2012.01.001

Soetanto, R., C.J. Hynes, H.R. Patel, D.T. Humphreys, M. Evers, G. Duan, B.J. Parker, S.K. Archer, J.L. Clancy, R.M. Graham, et al. 2016. Role of miRNAs and alternative mRNA 3′-end cleavage and polyadenylation of their mRNA targets in cardiomyocyte hypertrophy. *Biochim. Biophys. Acta.* 1859:744–756. https://doi.org/10.1016/j.bbagrm.2016.03.010

PLOS Genetics Staff. 2016. Correction: 3′UTR Shortening Potentiates MicroRNA-Based Repression of Pro-differentiation Genes in Proliferating Human Cells. *PLoS Genet.* 12:e1006254. https://doi.org/10.1371/journal.pgen.1006254

Steen, V.D., and T.A. Medsger Jr. 2000. Severe organ involvement in systemic sclerosis with diffuse scleroderma. *Arthritis Rheum.* 43:2437–2444. https://doi.org/10.1002/1529-0131(200011)43:11<2437::AID-ANR10>3.0.CO;2-U

Sun, M., J. Ding, D. Li, G. Yang, Z. Cheng, and Q. Zhu. 2017. NUDT21 regulates 3′-UTR length and microRNA-mediated gene silencing in hepatocellular carcinoma. *Cancer Lett.* 410:158–168. https://doi.org/10.1016/j.canlet.2017.09.026

Takagaki, Y., R.L. Seipelt, M.L. Peterson, and J.L. Manley. 1996. The polyadenylation factor CstF-64 regulates alternative processing of IgM heavy chain pre-mRNA during B cell differentiation. *Cell*. 87:941–952. https://doi.org/10.1016/S0092-8674(00)82000-0

Tashkin, D.P., R. Elashoff, P.J. Clements, J. Goldin, M.D. Roth, D.E. Furst, E. Arriola, R. Silver, C. Strange, M. Bolster, et al. Scleroderma Lung Study Research Group. 2006. Cyclophosphamide versus placebo in scleroderma lung disease. *N. Engl. J. Med.* 354:2655–2666. https://doi.org/10.1056/NEJMoa055120

Thomas, E., D.P. Symmons, D.H. Brewster, R.J. Black, and G.J. Macfarlane. 2003. National study of cause-specific mortality in rheumatoid arthritis, juvenile chronic arthritis, and other rheumatic conditions: a 20 year followup study. *J. Rheumatol.* 30:958–965.

Tian, B., and J.L. Manley. 2017. Alternative polyadenylation of mRNA precursors. *Nat. Rev. Mol. Cell Biol.* 18:18–30. https://doi.org/10.1038/nrm.2016.116

van den Hoogen, F., D. Khanna, J. Fransen, S.R. Johnson, M. Baron, A. Tyndall, M. Matucci-Cerinic, R.P. Naden, T.A. Medsger Jr., P.E. Carreira, et al. 2013. 2013 classification criteria for systemic sclerosis: an American College of Rheumatology/European League against Rheumatism collaborative initiative. *Arthritis Rheum.* 65:2737–2747. https://doi.org/10.1002/art.38098

Wang, Y., Y. Xu, W. Yan, P. Han, J. Liu, J. Gong, D. Li, X. Ding, H. Wang, Z. Lin, et al. 2018. CFIm25 inhibits hepatocellular carcinoma metastasis by suppressing the p38 and JNK/c-Jun signaling pathways. *Oncotarget*. 9:11783–11793.

Wu, M., D.J. Schneider, M.D. Mayes, S. Assassi, F.C. Arnett, F.K. Tan, M.R. Blackburn, and S.K. Agarwal. 2012. Osteopontin in systemic sclerosis and its role in dermal fibrosis. *J. Invest. Dermatol.* 132:1605–1614. https://doi.org/10.1038/jid.2012.32

Xia, Z., L.A. Donehower, T.A. Cooper, J.R. Neilson, D.A. Wheeler, E.J. Wagner, and W. Li. 2014. Dynamic analyses of alternative polyadenylation from RNA-seq reveal a 3′-UTR landscape across seven tumour types. *Nat. Commun.* 5:5274. https://doi.org/10.1038/ncomms6274

Xiang, Y., Y. Ye, Y. Lou, Y. Yang, C. Cai, Z. Zhang, T. Mills, N.Y. Chen, Y. Kim, F. Muge Ozguc, et al. 2018. Comprehensive Characterization of Alternative Polyadenylation in Human Cancer. *J. Natl. Cancer Inst.* 110:379–389. https://doi.org/10.1093/jnci/djx223

Yamamoto, T., and K. Nishioka. 2005. Cellular and molecular mechanisms of bleomycin-induced murine scleroderma: current update and future perspective. *Exp. Dermatol.* 14:81–95. https://doi.org/10.1111/j.0906-6705.2005.00280.x

Yamamoto, T., S. Takagawa, I. Katayama, K. Yamazaki, Y. Hamazaki, H. Shinkai, and K. Nishioka. 1999. Animal model of sclerotic skin. I: Local injections of bleomycin induce sclerotic skin mimicking scleroderma. *J. Invest. Dermatol.* 112:456–462. https://doi.org/10.1046/j.1523-1747.1999.00528.x

Zhou, X., F.K. Tan, X. Guo, and F.C. Arnett. 2006. Attenuation of collagen production with small interfering RNA of SPARC in cultured fibroblasts from the skin of patients with scleroderma. *Arthritis Rheum.* 54:2626–2631. https://doi.org/10.1002/art.21973

Zhu, Z.J., P. Huang, Y.X. Chong, L.X. Kang, X. Huang, Z.X. Zhu, and L. Nie. 2016. MicroRNA-181a promotes proliferation and inhibits apoptosis by suppressing CFIm25 in osteosarcoma. *Mol. Med. Rep.* 14:4271–4278. https://doi.org/10.3892/mmr.2016.5741

Supplemental material
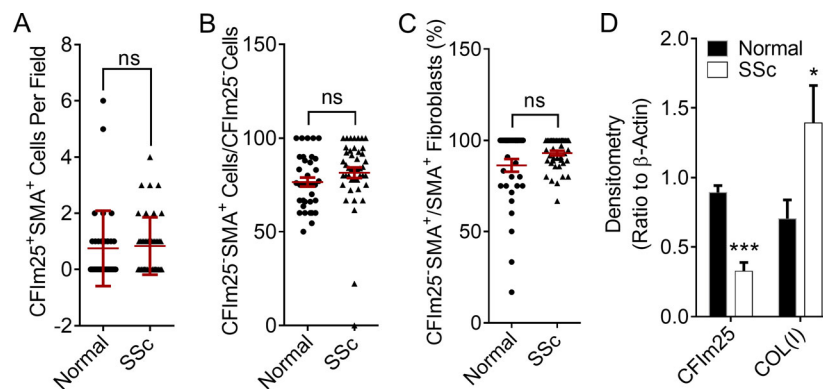
Figure S1. **Dual immunostaining was performed for CFIm25 and α-SMA expression in normal and SSc skin (*n* = 10). (A)** The number of CFIm25 and α-SMA double-positive cells was calculated for each sample. **(B)** The percentages of CFIm25⁻ and α-SMA⁺ cells in all α-SMA⁺ cells were counted and calculated. **(C)** The percentages of CFIm25⁻ and α-SMA⁺ cells in all CFIm25⁻ fibroblasts were counted and calculated. **(D)** The densitometry of CFIm25 and COL(I) were measured. P values were determined by a two-tailed Student's *t* test to determine the difference between normal and SSc cells. Data are presented as mean ± SEM and representative of two experiments with *n* = 10 per group (A–C) and two experiments with *n* = 5 per group (D). Data were analyzed using Student's *t* test. *, P < 0.05; ***, P < 0.001.
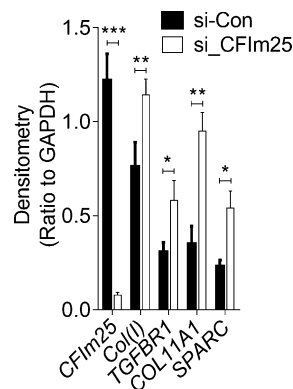

Figure S2. ***CFlm25* depletion induces upregulation of fibrotic factors in normal HDFs.** Five primary normal HDFs were transfected with *CFlm25*-specific siRNA (si_CFIm25) or a siRNA control (si_Con). Western blot were performed to confirmed effective *CFlm25* KD and increased protein levels of COL(I), TGFBR1, COL11A1, and SPARC. The densitometry of the Western blot was measured. Data are presented as mean (ratio to β-Actin) ± SEM and representative of three experiments with *n* = 5 cell lines per group. P values were determined using a paired two-tailed Student's *t* test comparing si_CFIm25 with si_Con. *, P < 0.05; **, P < 0.01; ***, P < 0.001.
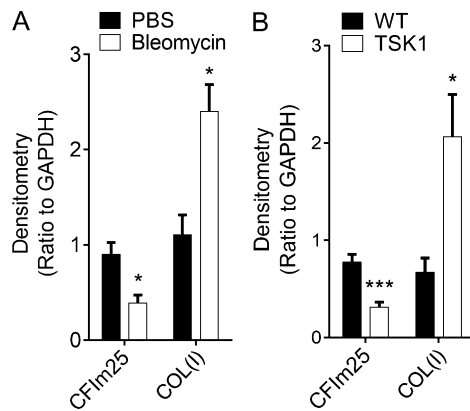
Figure S3. CFIm25 protein levels are decreased in murine models of dermal fibrosis. The densitometry of CFIm25 and COL(I) protein expression was determined in the skin lysate of (A) mice injected with PBS or bleomycin ($n = 3$ experiments with three or four mice per group) and (B) 8- to 10-wk-old WT and TSK1 mice ($n = 2$ experiments with six mice per group). COL(I) was used as a marker for fibrosis. Data are presented as mean (ratio to GAPDH) ± SEM. P values were determined using paired two-tailed Student's t test. *, $P < 0.05$; ***, $P < 0.001$.
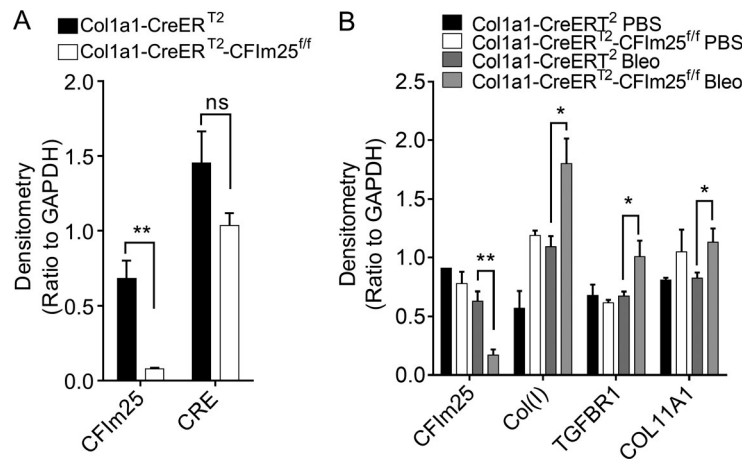
Figure S4. Knocking out *CFIm25* in fibroblasts promotes dermal fibrosis. 6- to 8-wk-old Col1a1-creER[T2] and Col1a1-creER[T2]-*CFIm25*[f/f] mice were treated with tamoxifen for 5 d to induce Cre activation. **(A)** Western blot was performed to determine Cre and CFIm25 expression in primary fibroblasts isolated from Col1a1-creER[T2]-*CFIm25*[f/f] mice ($n = 2$ experiments with four mice per group). Densitometry of the Western blot was measured and data were normalized to GAPDH. **(B)** Western blot was performed to confirm the downregulation of *CFIm25* and the upregulation of fibrotic makers in skin of PBS/bleomycin-treated Col1a1-creER[T2] and Col1a1-creER[T2]-*CFIm25*[f/f] mice ($n = 2$ experiments with approximately five to eight mice per group). Densitometry of the Western blot was determined. Data are presented as mean (ratio to GAPDH) ± SEM. P values were determined using an unpaired two-tailed Student's t test. *, $P < 0.05$; **, $P < 0.01$.
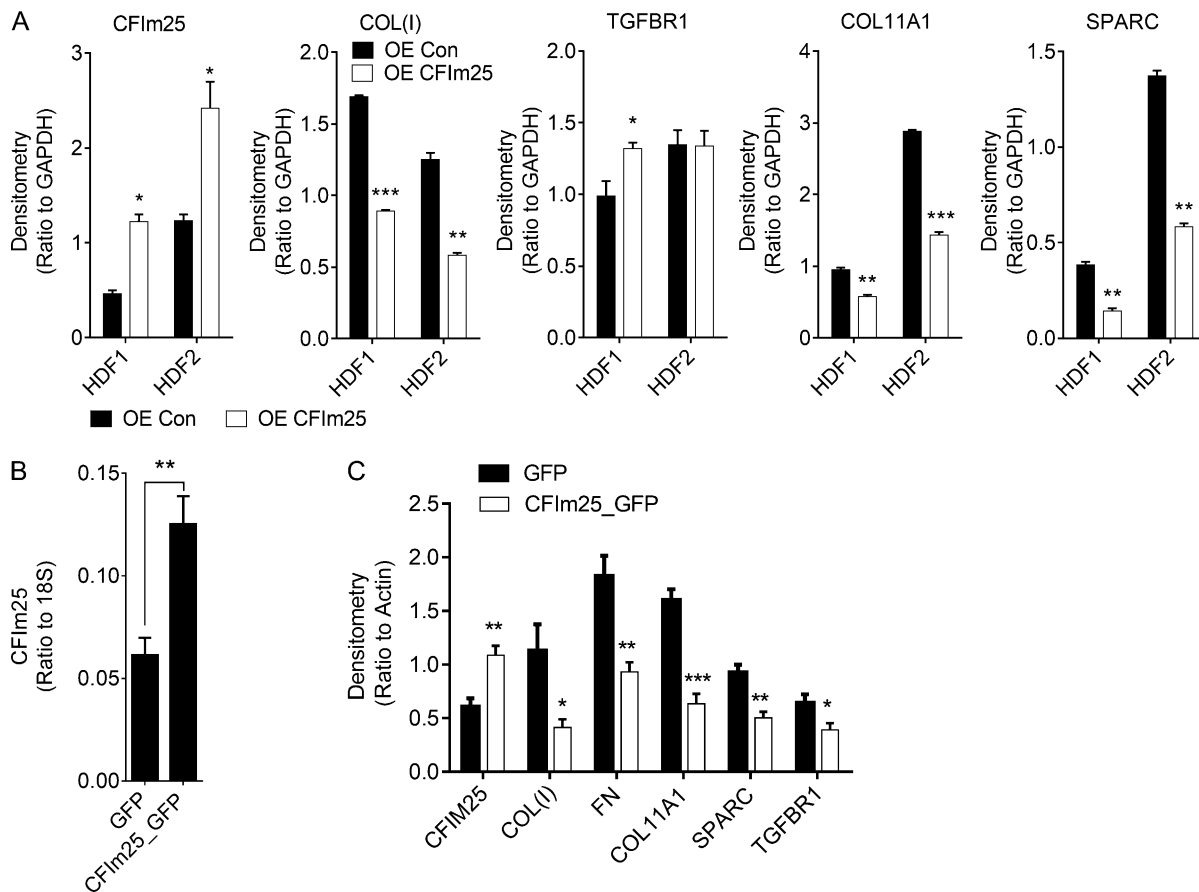
Figure S5. **CFlm25 OE attenuates fibrotic phenotype. (A)** Two HDFs were infected with control or *CFlm25*-overexpressing lentivirus at 25 MOI. Western blot was performed to confirm CFlm25 OE 2 d after the lentivirus infection and the expression of COL(I), TGFBR1, COL11A1, and SPARC 3 d after lentivirus infection. The densitometry of the Western blot image was quantified for each of the genes. **(B and C)** 6-wk-old mice were injected with s.c. GFP or CFlm25-IRES-GFP-overexpressing lentivirus (10×10^7 PFU/ml, 50 µl per spot) 1 wk before, 1 wk after, and 3 wk after the initial bleomycin injection. Then mice were injected with repeated s.c. bleomycin six times a week for 4 wk. Skin was collected 28 d after the initial bleomycin injection. **(B)** Subsequently, the *CFlm25* transcript levels were determined. **(C)** The densitometry of the Western blot image was determined to quantify the expression of CFlm25, COL(I), fibronectin (FN), TGFBR1, COL11A1, and SPARC. Data are presented as mean ± SEM for $n = 3$ experiments and two cell lines per group (A) or $n = 2$ experiments and five mice per group (B and C). P values were determined using an unpaired two-tailed Student's t test. *, $P < 0.05$; **, $P < 0.01$; ***, $P < 0.001$.

Table S1. **Demographic and clinical characteristics of participants in the immunohistochemistry experiments**

	SSc (*n* = 10)	Control (*n* = 10)
Age (yr), mean (SD)	41.18 (16.99)	45.15 (15.18)
Female gender, n (%)	6 (60%)	6 (60%)
Disease duration, mean (SD)	2.49 (0.94)	N/A
Skin score at the site of biopsy, mean (SD)	2.1 (0.32)	N/A
Overall modified Rodnan skin score, mean (SD)	26.7 (6.88)	N/A

N/A, not applicable.

Table S2. **Demographic and clinical characteristics of participants in the dPAS experiments**

	SSc (*n* = 10)	Control (*n* = 10)
Age (yr), mean (SD)	54.81 (7.94)	52.88 (7.7)
Female gender, *n* (%)	5 (50%)	5 (50%)
Disease duration, mean (SD)	1.18 (0.71)	N/A
Skin score at the site of biopsy, mean (SD)	2.3 (0.48)	N/A
Overall modified Rodnan skin score, mean (SD)	27.5 (5.54)	N/A

N/A, not applicable.

Table S3. **Primers used for RT-qPCR**

Gene	Forward primer (5′–3′)	Reverse primer (5′–3′)
Homo_CFIm25	TGAAGTTGAAGGACTAAAACGCT	ACCAGTTACCAATGCAATCGTC
Homo_COL1A1	GTGCGATGACGTGATCTGTGA	CGGTGGTTTCTTGGTCGGT
Homo_COL1A1 Long	GTGAGGGAGACAGACACCTG	GTGTTCTGGGGATTCAGGAG
Homo_TGFBR1	ACGGCGTTACAGTGTTTCTG	GCACATACAAACGGCCTATCTC
Homo_TGFBR1 Long	TTTGTGCAGGATTCTTTAGGCTT	GGCTTCTCAGTATCATTCGACTT
Homo_SPARC	TGAGGTATCTGTGGGAGCTAATC	CCTTGCCGTGTTTGCAGTG
Homo_SPARC Long	CAAGCCCAGCACTAGTCTCA	TGGTCTGCCTGCTAGAATGT
Homo_COL11A1	ACCCTCGCATTGACCTTCC	TTTGTGCAAAATCCCGTTGTTT
Homo_COL11A1 Long	TCTCCTTGTTTTCAGTGTGCTT	AGTCCACCATATGTTATTCATTTAGCA
Mus_COL1A1	GCTCCTCTTAGGGGCCACT	CCACGTCTCACCATTGGGG
Mus_COL1A1 Long	GGCAATGCTGAAATGTCCCA	ACAGTCCAAGAACCCCATGT
Mus_COL1A2	AAGGGTGCTACTGGACTCCC	TTGTTACCGGATTCTCCTTTGG
Mus_COL2A1	GGGAATGTCCTCTGCGATGAC	GAAGGGGATCTCGGGGTTG
Mus_TGFBR1	TCTGCATTGCACTTATGCTGA	AAAGGGCGATCTAGTGATGGA
Mus_TGFBR1 Long	TACGTCAGAAACACCATGGGA	ACAAAGGCCCCAAAAGTACC
Mus_FN1	GCTCAGCAAATCGTGCAGC	CTAGGTAGGTCCGTTCCCACT
Mus_ACTA1	GGCTGTATTCCCCTCCATCG	CCAGTTGGTAACAATGCCATGT
Homo_ACTA1	CATGTACGTTGCTATCCAGGC	CTCCTTAATGTCACGCACGAT